Journal of Techniques, ISSN: 2708-8383, Vol. 6, No. 4, 2024, Pages 1-18
DOI: https://doi.org/10.51173/jt.v6i4.2609

JOURNAL OF TECHNIQUES

Journal homepage: http://journal.mtu.edu.iq

RESEARCH ARTICLE - ENGINEERING (MISCELLANEOUS)

A Novel Rubber Composite Sleeper-Deformation-Prediction Model Based on Response Surface Method (RSM) and Machine Learning (ML) Techniques

Abdulmumin Ahmed Shuaibu[1*], Zhiping Zeng[2], Ibrahim Hayatu Hassan[3], Wang Weidong[2], Hassan Suleiman Otuoze[1], Suleiman Abdulhakeem[1], Bushrah Baba Abdulrahman[4]

[1]Department of Civil Engineering, Ahmadu Bello University, Zaria, Nigeria

[2]School of Civil Engineering, Central South University, Changsha, China

[3]Institute for Agricultural Research, Ahmadu Bello University, Zaria, Nigeria

[4]Department of Polymer and Textile Engineering, Ahmadu Bello University, Zaria, Nigeria

[*] Corresponding author E-mail: abdulshub4u@gmail.com

Article Info.

Article history:

Received
08 August 2024

Accepted
17 October 2024

Publishing
31 December 2024

Abstract

Rubber composite sleepers can experience significant temperature variations in service, causing temperature-induced deformation. Real-time monitoring of this deformation is crucial for operational safety and maintenance; however, it is costly, time-consuming, and requires substantial resources and personnel.
Developing temperature-dependent predictive models offers a cost-effective and efficient alternative, providing accurate insights into sleeper behaviour under different conditions while saving time, labour, and materials. This study attempts to develop a novel deformation model of rubber composite sleepers using response surface methodology (RSM) and machine learning (ML) techniques. Platinum temperature (Pt) sensors, embedded at various points on a full-scale rubber composite sleeper model, were used to measure both the sleeper temperature field and ambient temperature in real-time at 30-minute intervals over the period of a year. Simultaneously, lateral deformation was recorded using linear variable differential transducer (LVDT) displacement sensors. The temperature data were filtered to remove noise and normalized based on the Log-Pearson Type III outlier detection method and Box-Cox transformation, respectively, before being used to develop temperature-dependent models for sleeper deformation. To ensure accurate ML predictions, the dataset was split into 70% for training and 30% for testing. Model performance was evaluated using the correlation coefficient (R^2), mean square error (MSE), root means square error (RMSE), and mean absolute error (MAE). The analysis revealed that the sleeper's body temperature closely follows the changing trend of the ambient environment. Also, like any polymer material, the rubber composite sleeper expands when it absorbs heat from sunlight and contracts as it cools when sunlight intensity decreases, potentially reversing much of the deformation. The K-nearest neighbour algorithm outperformed the RSM and other ML techniques with R^2, MSE, RMSE, and MAE values of 0.999, 0.000258, 0.016, and 0.000896, respectively. The developed model can serve as an important reference for monitoring lateral deformation for safety and maintenance purposes.

Publisher: Middle Technical University

Keywords: Rubber Composite Sleeper; Deformation; Response Surface Methodology; Machine Learning; Temperature-Distribution.

1. Introduction

The popular materials used in the production of the vast railway sleepers already laid across the world are; timber, concrete, and steel which are generally designed for 20, 50 and 50 years, respectively [1-3]. Concrete sleepers are the most commonly used worldwide.

The oldest sleeper material is hardwood timber, with more than 2.5 billion wooden sleepers installed worldwide. Due to the scarcity of timber in many regions, its vulnerability to insect and weather damage, and environmental concerns surrounding the use and disposal of chemically-treated timber sleepers, the search for alternatives has become a global priority. Fig. 1 depicts a typical aged timber sleeper.

In the United States, for example, the prestressed concrete sleeper has been used to replace the timber sleeper, especially in heavy haul tracks to achieve superior stability, durability and strength capacity, resulting in reduced timber consumption, longer service life, lower maintenance costs, and increased eco-friendliness [4]. However, the concrete sleeper does not serve as a sustainable replacement for timber because replacing the vast number of timber sleepers worldwide with concrete sleepers is ineffective due to their larger size, heavier weight, higher stiffness, and incompatible mechanical properties [5, 8].

Nomenclature & Symbols			
RSM	Response Surface Methodology	ML	Machine Learning
Pt	Platinum Temperature	LVDT	Linear Variable Differential Transducer
MSE	Mean Square Error	RMSE	Root Means Square Error
MAE	Mean Absolute Error	R^2	Correlation Coefficien
ANOVA	Analysis of Variance	ANN	Artificial Neural Networks
RF	Random Forest	KLP	Kunststof Lankhorst Product
MPW	Mixed Plastic Waste	FFU	Fibre-reinforced Foamed Urethane
SVM	Support Vector Machine	BP	Backpropagation
HSRSBs	High-Speed Railway Suspension Bridges	TEMP	Considering Factors Such As Temperature
TDC	Time Delay Compensation	TLL	Train Live Load
TS	Train Side	TIP	Train Instantaneous Position

Currently, several polymer-based composite sleepers have been developed to serve as sustainable one-to-one replacements for timber sleepers. These sleepers were developed to mimic the behaviour of timber sleepers with superior resistance to environmental factors, longer service life and vibration mitigation characteristics. Most composite sleepers are made from recycled waste materials such as plastics, fillers, and bitumen, effectively reducing the volume of non-biodegradable waste that pollutes the environment. In addition to their environmental benefits, composite sleepers also provide a high strength-to-weight ratio, lower noise and vibration levels, and superior damping properties [9]. They are also resistant to bioerosion, fire, cracking, moisture, and insect or fungus attacks, while requiring minimal maintenance [10], thereby offering a range of technical, economic, and social benefits. However, they have low stiffness, low strength, and exhibit high plastic deformations under elevated temperatures [1]. To address the deficiencies in sleepers, reinforcements and modifications have been implemented to enhance their properties, thereby increasing their potential for broader application.

Several composite sleeper technologies have been developed in different parts of the world and are widely used in the United States, Australia, and Europe. However, in China, the use of this sleeper type is still limited. Composite sleepers can be classified by their properties and designated as type-1, type-2, and type-3 [11]. The following section discusses the types of composite railway sleepers.

Fig. 1. Aged timber sleeper [6]

1.1 Rubber/Polymer-Based Composite Sleeper

1.1.1. Sleepers with short or no fibre reinforcements (Type-1)

Type-1 sleepers are made from either recycled plastic materials (such as plastic bags, scrapped vehicle tyres, plastic coffee cups, milk jugs, and laundry detergent bottles) or bitumen combined with fillers like sand, gravel, recycled glass, or short glass fibres less than 20 mm [2]. Due to their short length, these fillers do not provide significant reinforcement, making the failure behaviour of these sleepers primarily polymer-driven. Additionally, these sleepers are highly flexible, causing them to expand and contract considerably with temperature changes, which leads to undesirable gauge widening [12]. The notable sleepers in this category are TieTek, Axion, IntegriCo, I-Plas, Tufflex, Natural Rubber, Kunststof Lankhorst Product (KLP), Mixed Plastic Waste (MPW), and Wood-core [2, 13-17].

1.1.2. Sleepers with long fibre reinforcement in the longitudinal direction (Type-2)

The Type-2 sleepers are reinforced with continuous glass fibres extending longitudinally while having either no fibres or very short random fibres in the transverse direction. [10]. Long glass fibres primarily govern the strength and stiffness in the longitudinal direction, while the polymer dominates the transverse direction. These sleepers are mainly suitable for ballasted rail tracks, where stresses in the sleepers are governed by flexural loading. However, they are less ideal for bridge applications where the sleepers are subjected to high levels of combined flexural and shear forces [2, 12]. The FFU (Fibre-reinforced Foamed Urethane) synthetic sleeper is classified in this sleeper category [2, 18].

1.1.3. Sleepers with fibre reinforcement in longitudinal and transverse directions (Type-3)

Type-3 sleepers incorporate long reinforcement fibres oriented in both the longitudinal and transverse directions, leading to fibre-dominant flexural and shear behaviour. The structural performance of these sleepers can be engineered by adjusting the fibre reinforcements in each

direction to meet specific performance requirements. [10]. This category includes sandwich polymer sleepers (e.g., glue-laminated sandwich composite) and hybrid composite sleepers (e.g., geopolymer concrete-filled pultruded composite) [2].

The performance of the three types of composite sleepers relative to timber sleepers is presented in Table 1.

Table 1. The performance of the composite sleepers

Performance measurement	AREMA Specification			Type-1	Type-2	Type-3
	Oak	Softwood	Glulam			
Density, (kg/m^3)	1096	855	960	850-1150	740	1040-2000
Modulus of elasticity, (GPa)	8.4	7.4	12.0	1.5-1.0	18.1	5.0-8.0
Modulus of rupture, (MPa)	57.9	49.3	66.9	17.2-20.6	142	70-120
Shear strength, (MPa)	5.0	4	4	54	10	15-20
Rail seat compression, (MPa)	4.6	3	3.9	15.2-20.6	28	40
Screw withdrawal, (kN)	22.2	13.3	n/a	31.6-35.6	65	> 60

(Adopted from Ferdous et al., [2, 19]; Shanour et al [20])

Several Static and dynamic tests have been conducted on these different sleepers using experimental methods and numerical calculations, with the results well documented in the literature. For instance, Zeng et al. [21], Zeng et al. [22, 23], Zhao et al. [24, 25], Jabu et al. [26], and Zhao et al. [27] investigated the vibration reduction characteristics and dynamic behaviours of rubber composite sleepers. Meanwhile, the static flexural properties of various composite sleepers have been explored by researchers such as Lotfy et al. [5], Lojda et al. [28], Lofty et al. [29], Yu et al. [30], Siahkouhi et al. [31], and Salih et al. [32].

Considering the nature of the materials used in composite sleepers, their properties can become polymer-driven when exposed to temperature fluctuations during service conditions. The surface and internal temperature variations could lead to temperature-induced deformations. When these deformations are restricted by boundary conditions, temperature-induced loading can occur, potentially leading to issues such as crack formation, plastic deformation, upwarping, and other defects [33]. Additionally, the sleeper's temperature is expected to closely follow that of its surroundings and with the rising air temperatures due to global warming, the risk of composite sleeper deformation increases. These problems negatively affect the safety, performance, stability, and strength of the track, while also raising maintenance costs. Currently, there is quite limited study on the temperature-induced deformation of the polymer/rubber composite sleeper and to the best knowledge of the authors, there are no well-defined limits for the deformation of composite sleepers in a natural environment. Developing accurate temperature-dependent predictive models offers a more cost-effective and efficient alternative, providing accurate insights into sleeper behaviour under different temperature conditions while saving time, labour, and materials.

In recent years, statistical approaches such as response surface methodology (RSM), and machine learning (ML) approaches such as artificial neural networks (ANN), random forest (RF), support vector machine (SVM), and extreme gradient boosting (XGBoost) have emerged as widely used techniques for efficiently modelling high-dimensional and non-linear processes in the field of Civil Engineering. ML is widely used for engineering predictions due to its ability to learn from experimental/sample datasets (training data).

Response surface methodology (RSM) has been widely employed for modelling, prediction, and optimization in various research areas, including cement concrete [34-41], asphalt concrete [42-45] and railway engineering [46-48] consistently yielding reliable results as reported in the literature. Meanwhile, machine learning techniques have also gained extensive application across numerous fields, providing advanced capabilities for data analysis and optimization. For instance, using machine learning techniques, Liu et al. [49], proposed a deformation prediction based on a backpropagation (BP) neural network for High-speed railway suspension bridges (HSRSBs) considering factors such as temperature (TEMP), time delay compensation (TDC), train live load (TLL), the train side (TS) and train instantaneous position (TIP). The model was evaluated using a dataset of 10-day field measurements. They concluded that the model is highly accurate with a high coefficient of determination (R^2) and low error margin. Also, Ramos et al. [50] employed five ML algorithms; multivariable regression, decision tree, random forest, ANN and SVM to predict the permanent deformation and respective settlement of railway track. Model performance was evaluated using standard metrics such as correlation coefficient, root mean square error etc. They found that the random forest model showed the best performance. Considering field data from four different sites, Chen et al. [51] developed a frost heave deformation predictive model based on an artificial neural network and long-short-term memory (LSTM) for the high-speed railway subgrade. The results indicate that the LSTM model, configured with 12 hidden neurons, achieves optimal performance with a reduced number of parameters. It records an average RMSE of 0.0210 mm and an MAE of 0.0138 across all training samples, demonstrating that the model exhibits high precision in this specific scenario. Kaewunruen et al. [52] employed four different machine learning techniques namely, deep learning, Bayesian neural network, and random forest to investigate the potential of machine learning to predict the capacity of railway prestressed sleepers using a large design data set. Based on solar and weather data, Hong et al. [53] predicted rail-temperature using traditional statistical methods and machine learning techniques such as extreme gradient boosting (XGBoost), support vector machine (SVM), random forest (RF), artificial neural network (ANN) and second-order polynomial (PR^2). Indraratna et al [54] employed an artificial neural network (ANN) and adaptive fuzzy inference system (ANFIS), to predict the resilience modulus of ballast material with loading magnitude, cycle, frequency and confining pressure as explanatory variables. Aela et al. [55] utilized four classification algorithms such as support vector machine (SVM), back propagation neural network (BRNN), random forest (RF) and Catboost (CB) to predict ballast particle number after breakage with size and shape of particles, material properties and loading conditions as input variables.

Although lots of studies have employed the RSM and ML for modelling and prediction, there are still very limited studies on the modelling of the deformation of polymer-based composite sleepers (herein referred to as rubber composite sleepers) under environmental temperatures.

The current study seeks to develop a novel-rubber composite sleeper (type-1) deformation model based on sleeper body temperatures using the response surface method and machine learning techniques. In an attempt to achieve the aim of the study, the sleeper temperature-field variation and that of the ambient environment were collected. Also, the correlation of the sleeper temperature (internal and surface) with that of the ambient and deformation was obtained. The seasonal variation of the sleeper deformation was presented by selecting typical days in each season. Furthermore, the response surface method (RSM), XGBoost, CatBoost, and RF regression tool were employed to predict the deformation of the rubber composite sleepers while considering the average internal and external sleeper temperatures as input variables. The

performance of the models developed was evaluated using coefficient of determination (R^2), mean squared error (MSE), root mean square error (RMSE), and mean absolute error (MAE). To meet the split requirements of the datasets in ML prediction, the authors relied on the body of literature to enable them to arrive at a split that will give an optimum prediction,

The novelty of this study is that the developed models can significantly reduce the time, energy and cost required for expensive experimentation as well as serve as a guide to monitor/check the deformation of the rubber composite sleeper under service conditions for safety and maintenance.

2. Materials and Method

2.1. Materials

The experimental set-up in this study consists of the rubber composite sleeper, the pt. 100 temperature sensors, a data acquisition device and a computer. The rubber composite sleeper was supplied by Tianjin Yanwen Weiye Plastic Product Cooperation, Tianjin, China. The geometrical characteristics as well as performance properties are shown in Table 2.

Table 2. Dimensional and Properties of Rubber Composite Sleeper from Laboratory Experiments

Properties	Length (m)	Width (m)	Depth (m)	Mass (Kg)	Gauge (m)	Density (Kg/m^3)	Modulus of Elasticity (MPa)
Rubber composite sleeper	2.5	0.22	0.16	125	1.435	1397	1552

Pt 100 which is considered as reliable and accurate device for measuring temperature [56] was used to collect temperature measurements at the sleeper surfaces (top, bottom, left side and right side) and from 55mm depth from the surfaces.

The sensor was developed by Huaian Sen Ling Instrument Co Ltd, China following DIN/IEC 60751 (or simply IEC751) standards. The data acquisition system used in this study is the JM3812 multifunctional static strain gauge developed by Yangzhou Jingming Technology Co., Ltd, in China. The data acquisition system served as a bridge between the sensors and the computer. A Windows-based powerful software (JMTest) installed in the system was used for visualizing the data measurement and acquisition. The computer has the specification as follows; Windows 10, 64-bit with, 16 GB RAM, high-speed USB port, Intel ®, core ™ i5-4200U @ 2.30GHz was used to acquire the data.

2.2. Full-scale experimental model with the arrangement of sensors for measuring temperature field and deformation

To achieve the connections necessary for the collection of temperature-field distribution as well as resulting deformation in the rubber composite sleeper, one end of the temperature sensor was placed at the surfaces and 55mm depth from the surfaces (top, bottom, left side, and right side), and the other ends of each sensor was connected to the data acquisition device which was ultimately connected to a computer. In contrast, the ambient temperature was collected by placing one end of the sensor in the data acquisition device and the other end in an open box. Added to the temperature collection set-up is the linear variable differential transducer (LVDT) displacement sensor that was used to collect the lateral deformation of the sleeper on both ends of the sleeper (left and right positions). Both temperature distribution and deformation were collected (at 30-minute intervals) through the data acquisition device on the computer in real-time (see Fig. 2). Windows-based powerful software (JMTest) is installed in the system to visualize the data measurement and acquisition. A Windows 10, 64-bit computer with, 16 GB RAM, high-speed USB port, Intel ®, core ™ i5-4200U @ 2.30GHz was used to acquire the data.

The temperature data was collected for one year (09/10/2019 to 09/10/2020), making a total of 15,764 readings per sensor, except where there are system/power failures. The experimental set is shown in Fig. 2. The temperature of the inner and outer surfaces of the sleeper with their corresponding deformation served as the basis for the development of temperature-dependent lateral deformation models of the rubber composite sleeper.

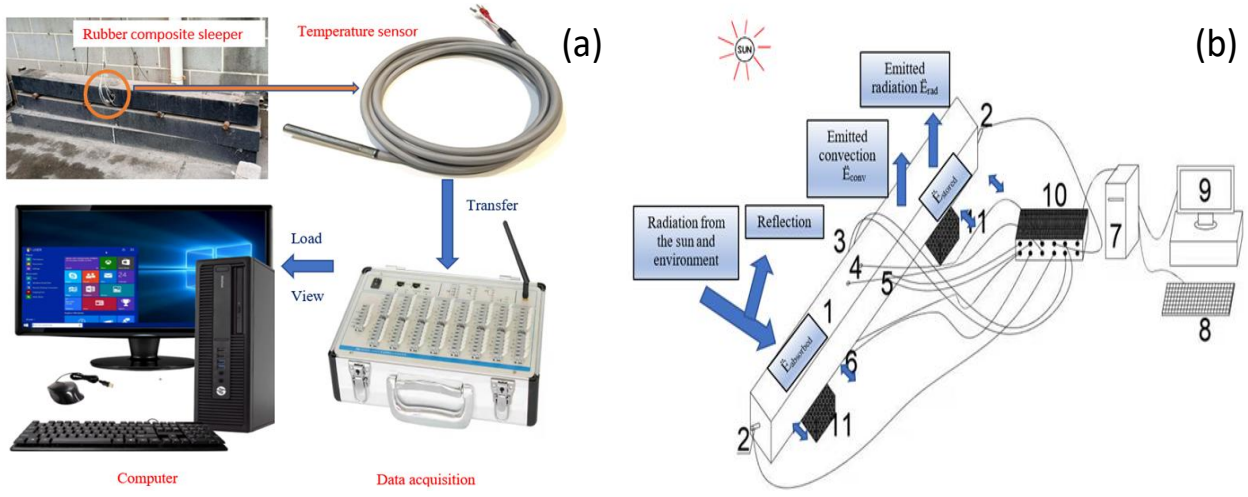

Fig. 2. Experimental set-up; (a) the measurement system, (b) the sensor arrangement

Where; 1- Rubber composite sleeper, 2- LVDT sensor, 3- Temperature sensor placed on the left side surface and at 55mm depth from the left side, 4 - Temperature sensor placed on the sleeper top surface and at 55mm depth from the top, 5 - Temperature sensor placed on the right-side surface and at 55mm depth from the right side 6 - Temperature sensor placed on the sleeper bottom surface and at 55mm depth from the bottom, 7- Computer central processing Unit (CPU), 8- Computer keyboard, 9- Computer monitor, 10 - Data acquisition device 11- support.

2.3. Development Temperature-dependent lateral deformation of rubber composite sleeper

2.3.1. Data collection and Model Structure

The 15,764 individual rubber composite sleepers body temperatures obtained from laboratory experiments over on year were filtered to remove noise and normalized based on the Log-Pearson Type III method of outlier detection method and Box-Cox transformation respectively. The clean and normalized dataset was used to develop temperature-dependent models of sleeper deformation via different algorithms; Response Surface Methods (RSM), CatBoost, Random Forest, XGBoost and K-nearest neighbour. Consequently, a total of 10,609 datasets were used for model development.

The identification of outliers using the Log-Pearson Type III method can detect both low and high outliers. The high and low outliers in the dataset were determined using Equations 1 and 2 respectively:

$$Y_L = \acute{Y} + K_N S_Y \quad (1)$$

$$Y_L = \acute{Y} - K_N S_Y \quad (2)$$

Where Y_L is the log of high or low outlier limit, $\acute{Y}$ is the mean of the log of the sample flows, S_Y is the standard deviation of the logs of the sample flows and K_N is the critical deviate of the data set.

The Box-Cox transformation is applied to models/datasets that deviate significantly from a normal distribution or have high skewness, kurtosis, and heteroscedasticity. The Box-Cox transformation, however, helps to satisfy the assumptions of normality, improves the performance of the models by reducing heteroscedasticity, and makes it easier to interpret the model results. The Box-Cox transformation equations are shown in Equations (3) and (4).

$$y_i^{(\lambda)} = x_i'\beta + \in_i,\ i = 1, \dots \dots, n, \quad (3)$$

Where

$$y_i^{(\lambda)} = \begin{cases} \frac{(y_i^{\lambda}-1)}{\lambda}, & \lambda \neq 0, \\ \log y_i, & \lambda = 0, \end{cases} \quad (4)$$

$y_i^{(\lambda)} =$ is called the Box-Cox transformation of y_i, $\beta = (\beta_0, \cdots, \beta_{p-1})$ is the p-dimensional vector of unknown regression coefficients, and $\in_i$ is an error term independently following $N(0, \sigma^2)$.

The descriptive statistics of the temperature and deformation data, experimentally collected and used for model development, are shown in Table 3.

Table 3. Descriptive statistics for input and output parameters used in model development

S/No	Parameters	Units	Role	Minimum value	Maximum value	Mean	Standard deviation
1	Top surface	^{0}C	Input	1.580	44.600	21.604	10.546
2	Bottom surface	^{0}C	Input	2.421	48.100	20.897	8.898
3	Left surface	^{0}C	Input	1.325	43.210	24.398	13.630
4	Right surface	^{0}C	Input	1.500	42.500	21.657	10.025
5	55mm from the top surface	^{0}C	Input	1.753	47.000	20.883	9.077
6	55mm from the bottom surface	^{0}C	Input	1.545	43.567	23.100	10.180
7	55mm from the left surface	^{0}C	Input	1.980	45.336	21.758	10.353
8	55mm from the right surface	^{0}C	Input	1.346	45.336	21.236	10.336
9	**Deformation**	mm	Output	-4.805	6.073	0.3630	1.752

To develop the prediction equations for the temperature-dependent deformation of rubber composite sleeper, the sleeper body temperature and their corresponding lateral deformation collected in the experiment were used. It should be noted that the sleeper body temperature both inner and surface (as in Table 2) showed a consistent/similar trend. The same trend/result was obtained between the sleeper's body temperature and the ambient. On this note, the average of the inner and surface temperatures at all measuring points have been aggregated to represent the inner and surface temperature of the sleeper respectively. Thus, to simplify the model, an average of inner and surface temperature was considered. The objective behind this modelling process is that it can serve as a quick guide and reference for knowing the maximum sleeper deformation once the ambient (from measuring stations) or sleeper body temperature is known.

The model is expected to result in significant savings in terms of testing time, technician and equipment costs, as well as data processing and analysis time. Mathematically, the developed equation has the following structure:

$$Def_{sleeper} = (T_s, T_i) \quad (5)$$

Equation 1 shows that the rubber composite sleeper deformation is a function of average surface temperature; T_s and average internal , T_i.

2.4. Statistical modelling using RSM and machine learning

2.4.1. Response surface method (RSM)

The response surface method (RSM) introduced by Box and Wilson in 1951 is a powerful statistical tool for optimum condition search, model construction, factor effect analysis, and experimental design [35]. The method is specifically known for establishing a relationship/implication between input variable(s) on output(s)/response via a statistical approach using regression equations as presented in Equation (6).

$$y = \beta_0 + \sum_n^k \beta_i x_i + \sum_n^k \beta_{ii} x_i^2 + \sum_n^k \beta_{ij} x_i x_j + \in \quad (6)$$

Where y is the dependent variable (deformation), β_0 is a constant coefficient, β_i, β_{ii} and β_{ij} are the regression coefficients for linear, quadratic and interaction terms, respectively, x_i and x_j are the independent variables (internal and surface sleeper temperature), while $\in$ is the error.

The model terms were selected based on a 95% confidence level and the consistency of the model fit based on the regression coefficient (R^2). Validation was carried out using adequate precision (signal-to-noise ratio) and agreement between the adjusted R^2 and the predicted R^2. Finally, based on the interactive effect between the independent variables, i.e., surface and internal temperatures, the 2D and 3D plots were generated for verification. The RSM Design Expert version 13 statistical package was used to implement the prediction in this study.

2.4.1. Machine Learning (ML) method

For the ML modelling, the sleeper body temperature (average inner and surface) was treated as the explanatory variable (two variables) while the deformation was the response variable.

In the current study, 70% (7420 data points) and 30% (3180 data points) of total data points were assigned to the training/model construction dataset and testing/validation dataset, respectively similar to the previous related study [57].

In this study, the selected machine learning techniques are random forest (RF), CatBoost, extreme gradient boost (XGBoost), and K-nearest neighbor (KNN). The flowchart of the machine learning procedure implemented in this study is presented in Fig. 3.

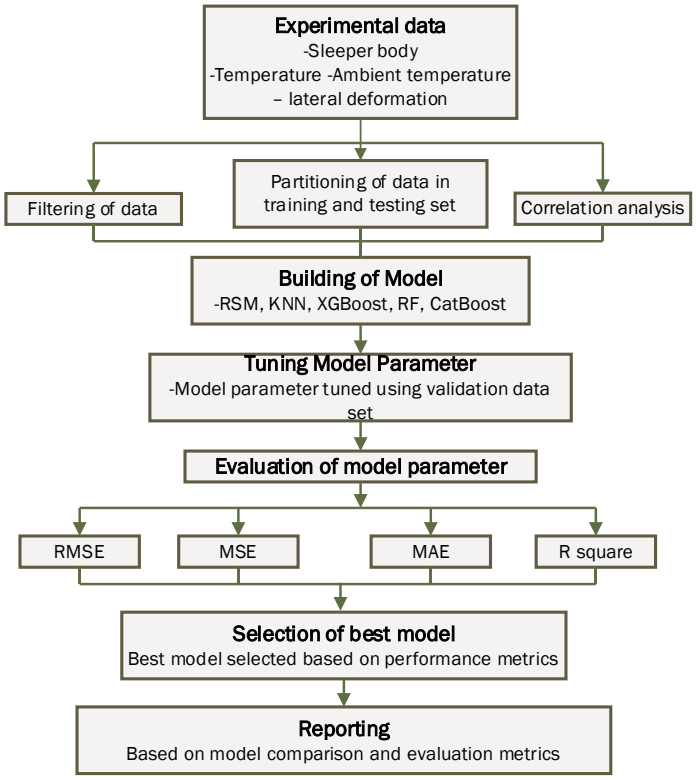

Fig. 3. Flow chart of machine learning procedure implemented in this study

The following section gives a detailed explanation of the methodology employed to achieve the result of the ML predictions.

2.4.2. Random Forest (RF)

A regression method called random forest is an advanced version of bagging that combines the effectiveness of numerous decision tree algorithms to predict variable values [58]. The random forest method is one of the most practical methods of ensemble learning [58] and it applies to both linear and nonlinear data in regression and classification problems.

In the random forest process, an algorithm is used to construct a decision tree in the forest for each training dataset (Fig. 4). Thus, several decision trees (predictions) are developed and the final RF prediction model is based on an average of the decision trees utilizing the most popular approach [59] thus, making it less prone to overfitting. The averaging for regression application is based on Equation (7) [60].

$$f(x) = \frac{1}{J}\sum_{j=1}^{J} h_j(x) \tag{7}$$

Herein, $h_j(x)$ refers to the set of base learners.

The optimized hyperparameters used for RF in this study are as follows; n_estimators = 590, min_samples_split = 14, min_samples_leaf = 3, max_features = auto', max_depth = 17.

2.4.3. Extreme Gradient Boosting (XGBoost)

XGBoost refers to an ensemble of classification and regression (CART) [61]. It belongs to the category of efficient gradient-boosted trees that minimize search space for possible feature splits by utilizing the feature distribution across all data points in a leaf [62].

At each iteration, the algorithm produces a weak learner and accumulates it into the overall model. If the weak learner corresponds to the gradient direction of the loss function, then, the learning method is called a gradient-boosting machine [61]. XGBoost is well recognized for its scalability, parallelization, optimization capacities and accuracy [63]. Detailed explanations of the XGboost algorithms can be found in other works of literature such as that of Chen and Guestrin [64]. However, the loss of function can be expressed mathematically as presented in Equation (8) [65].

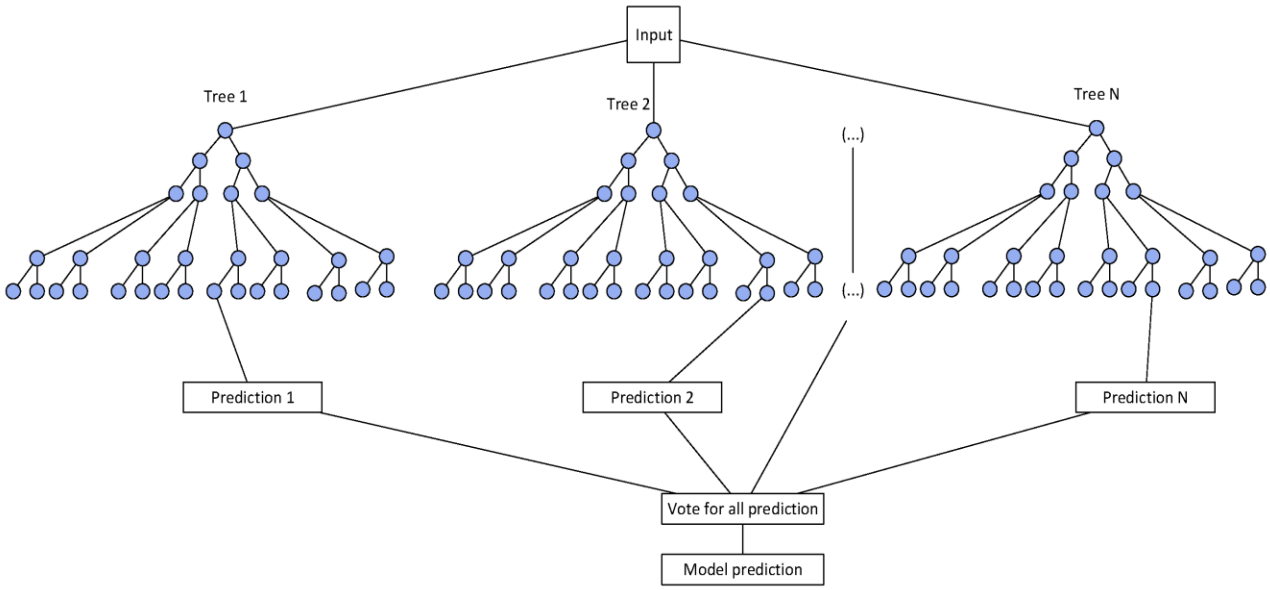

Fig. 4. The architecture of the RF

$$\sum_{j=1}^{T_m} L = [G_{jm}w_{jm} + \frac{1}{2}(H_{jm} + \lambda_R)w_{jm}^2 + \alpha_R|w_{jm}|] + \gamma T_m \quad (8)$$

Here, L represents the loss function, α_R and λ_R refer to the L_1 and L_2 regularization terms respectively. γ denotes the Lagrangian multiplier also known as the penalty terms, H_{jm} s sum of hessian used to estimate the least number of child weights and G_{jm} is the sum of the gradient. T_m and w_{jm} refer to optimal weights and leaves trees over maximum depth $D_{max.}$

The optimized hyperparameters used for XGBoost in this study are as follows; lambda = 1.0, alpha = 0.001, n_estimators = 300, max_depth = 9, learning rate = 0.01, gamma = 0.22222.

2.4.4. K-nearest neighbor (KNN)

The K-Nearest Neighbor (KNN) is a supervised ML algorithm used for nonlinear regression. It can predict unseen data (testing data) by sorting and finding the data points closest to the training dataset, thus referred to as nearest neighbours [66]. The KNN algorithm utilizes a distance function, typically, the Euclidean function, for continuous variables to measure the similarity between training and testing datasets [67].

The KNN algorithm suggests that data with similar trends will cluster together within a space, thus enabling the identification of K nearest points to the input data under investigation. Consequently, the algorithm makes decisions based on nearest point information [67].

To evaluate the Euclidean distance between each unknown data point and the sample plot, Equation (9) was employed.

$$\gamma = \sqrt{\sum_{k=1}^{m}(u_k - v_k)^2} \quad (9)$$

γ represent the spectral distance between the u and v in n-dimensional space, u_k and v_k represent the spectral values of the unknown variable and v in the Kth selected spectral variable, respectively.

Through a trial-and-error process, the following hyperparameters were used in the optimized KNN model: weights = 'distance', p = 2, n_neighbors = 14, algorithm = ball_tree.

2.4.5. CatBoost

Catboost is a supervised ML technique based on the gradient-boost decision tree method [68]. It can handle nonlinear datasets, missing data, and categorical data. Furthermore, it has a strong learning capacity [69].

It brings together two boost modes, namely; ordered target statistics and ordered boosting [70]. ‘‘The plain mode is the traditional gradient boosting decision tree (GBDT) algorithm which incorporates an ordered target statistic [65] while the ordered boosting as described by Prokhorenkova et al. [71] is an effective modification of the ordered-boosting algorithm.

The Catboost algorithm employs decision trees as a base weak learner and fits the gradient boosting sequentially to the decision tree [72]. Through gradient descent (Equation 10), each new tree is expected to exhibit a lower loss than the prior trees [68, 73].

$$h^t = arg_{h\in H} min \mathrm{E}\ \{\mathrm{L}\ (\mathrm{y}, F^{t-1}(x) + h(x))\ \} \quad (10)$$

Herein y denotes the output, and h represent a gradient step function selected from H, a family of functions. Furthermore, the step function can be calculated using Equation (11)

$$\boldsymbol{h(x) = \sum_{j=1}^{J} b_j \, \|_{\{x \epsilon Rj\}}} \tag{11}$$

Herein, R_j represent the disjointed region that corresponds to tree leaves while b_j represent the predictive value of the region, and $\|$ is an indicator function.

In the CatBoostRegressor, the following parameters were considered: n_estimators = 650, max_depth = 7, and learning_rate = 0.01 to improve model performance.

2.5. Hyperparameter tuning by K-Fold cross validation

In the field of machine learning, the performance is largely influenced by the values of the hyperparameters and this is referred to as tunning. The appropriateness of the value range of the hyperparameter(s) relies to a great extent on the user's intuition and experience.

In this study, the GridSearchCV function in the Python library Scikit-learn was used considering the size of the dataset to obtain the best set of hyperparameters. The GridSearchCV utilized a default of 3-fold cross-validation (k=3); however, to optimize the accuracy of the hyperparameter combination in this study, a k value of 5 was used. A k value of 5 implies that the data set was randomly split into 5 subgroups and at each time one of the subgroups was used to validate the model while the other 4 were used for model development (training). This allows for improved model accuracy and fewer tendencies for overfitting. Thus, the optimized parameters used to obtain high-performance models for each of the machine-learning languages are as follows.

2.6. Evaluation of Model Performance

To assess the performance of the developed models, different indicators such as correlation coefficient (R^2) and Root mean squared error (RMSE) [74-78] were used.

2.6.1. Mean Square Error (MSE)

Mean square error (MSE) equation 12 is an error metric that measures the appropriate standard deviation of the relative error margin between the experimental/measured and the predicted value in modelling [72].

$$MSE = 1 - \frac{\sum_1^n (P_i - M_i)^2}{N} \tag{12}$$

2.6.2. Root Mean Squared Error (RMSE)

Root Mean Squared Error (RMSE) (Equation 13) is a commonly used error metric in modelling studies. It is the square root of mean square error (MSE) - a statistical estimator that measures the average of the squares of the errors between the observed and predicted values. Here, the prediction errors are quantified in terms of the units of the variables calculated by the model [78]. The value ranges from zero to infinity, and an RMSE is zero (0) indicates a perfect fit. The RMSE value can be calculated as follows [79-82]:

$$RMSE = \sqrt{\frac{\sum_{i=1}^n (P_i - M_i)^2}{N}} \tag{13}$$

Where P and M are the predicted and measured deformations, and n is the number of input samples.

2.6.3 Coefficient of determination (R^2)

The coefficient of determination (R^2) (Equation. 14) is the square of Pearson's product-moment correlation coefficient. This measures the degree of collinearity between simulated and observed data [78]. The accuracy of a model is defined by its coefficient of determination (R^2). For the effective model, its value should be close to 1, and a value greater than 0.8 presents a high accuracy of the model [83]. An R^2 value close to 1 and lower values of errors (MAE, RRMSE, RMSE, and RSE) indicate higher accuracy of the model [77]. The R^2 value can be calculated as follows [84]:

$$R^2 = \frac{\sum_1^n (M_i - M_{iavg})\,(P_i - P_{iavg})}{\sqrt{\sum_1^n (M_i - M_{iavg})^2 \sum_1^n (P_i - P_{iavg})^2}} \tag{14}$$

Where P is the predicted deformation, M is the measured deformations, M_{iavg} average measured deformation, P_{iavg} is the average predicted deformation and n is the number of input samples

2.6.4. Mean Absolute Error (MAE)

Mean Absolute Error (MAE) is a model evaluation metric used with regression models. The mean absolute error of a model concerning a test set is the mean of the absolute values of the individual prediction errors over all instances in the test set [85]. The Mean absolute error (MAE) score is measured as the average of the absolute error values. The Absolute is a mathematical function that makes a number positive. Therefore, the difference between an expected and predicted value can be positive or negative and will necessarily be positive when calculating the MAE [86]. The MAE value can be calculated as follows[79-82]:

$$MAE = \frac{\sum_{i=1}^n |P_i - M_i|^2}{N} \tag{15}$$

Herein, P is the predicted deformation, M is measured deformations, and n is the number of input samples.

For model performance evaluation, generally, a high R2 and a lower error metric are considered desirable.

3. Results and Discussions

This section presents the results of temperature-field variation on the rubber composite sleeper. Also, the results of temperature-dependent deformation of the sleeper using different prediction methods were presented and evaluated. Finally, the model that best predicts the deformation of the rubber composite sleeper was selected based on the performance evaluation criteria highlighted in section 2.4.

3.1. Temperature variation of rubber composite sleeper under natural temperature conditions

Fig. 5(a) presents the temperature-field variation of the rubber composite sleeper at surfaces (top, bottom, left and right) and 55mm depth from the surfaces (internal). The result shows that due to the effect of direct solar radiation and convective heat transfer, the sleeper body (surface and at 55mm depth) temperature field exhibited a similar and consistent changing pattern over different seasons with very insignificant differences.

A similar trend was observed between the sleeper body temperature (both surface and internal) and those of the ambient/environmental conditions. To further elucidate the similarity of the trend of the sleeper body temperature-field and the environment, the average internal and surface temperature of the rubber composite sleeper was compared to those of the ambient temperature as presented in Fig. 5(b) and results further confirm the observation in Fig. 5(a). The very little difference between the surface and the inner temperature is an indication of no or recoverable temperature-induced deformation of the sleeper during the testing period of one year.

This result agreed with the AREMA manual which states ‘‘that dimensional changes in the composite sleeper do not occur instantaneously with the change in ambient temperature’’. It should be noted that the sleeper's ambient environment has a significant influence on the temperature-field distribution of the sleeper, thus, the ambient temperature can substitute the sleeper’s body temperature where the luxury of cost and time isn’t readily available.

To further explore the relationship between the internal/external temperature with ambient as well as deformation, correlation analysis was performed to measure the strength of the relationship/association between them and the result is presented in Fig. 6.

According to Fig. 6(a) and (b), there is a significant positive association between the surface and ambient temperatures (correlation coefficient = 0.968) and between the internal and ambient temperatures (correlation coefficient = 0.983). This suggests that the surface and internal temperatures rise or fall as the outside temperature does. As a result, the ambient temperature is responsible for roughly 96.8% and 98.3% of the sleeper's surface and internal temperatures, while 3.2% and 1.7% of those temperatures can be attributed to the sleeper's material type, resistivity, humidity, conduction, etc. The close relationship or correlation between the ambient temperature and the internal or surface temperature of the sleeper suggests that, in the absence of the sleeper's body temperature, the ambient temperature present in the meteorological station can be relied upon to provide a highly accurate prediction of sleeper deformation. However, the two factors considered for prediction in this study are the average surface and internal temperatures collected during the one-year experiment.

The results from Fig. 6(c) and (d) show that there is a fair positive correlation between the sleeper’s internal/surface temperature and the sleeper’s deformation. Also, the Fig. 6 showed that the sleeper's internal temperature contributes more to the sleeper’s deformation compared to the surface temperature.

3.2. Seasonal variation of the lateral deformation of rubber composite sleeper

To explore the deformation properties of the rubber composite sleeper over different seasons, typical days in each season were considered and the plot is presented in Fig. 7. According to Fig. 7, the left, right and total deformation of the rubber composite sleeper showed similar and consistent trends. The deformation of the rubber composite sleepers gradually increases as the ambient temperature increases and vice versa. On a general note, the deformations of the sleeper decrease with a decrease in sunlight intensity from nightfall until they reach their maximum negative value at midnight and the early hours of the day. Then, they begin to gradually increase after daybreak with an increase in the intensity of the sunlight until they reach their maximum positive value. After which it begins to decrease again. This cycle continues daily without exceeding the elastic limits of the sleeper material.

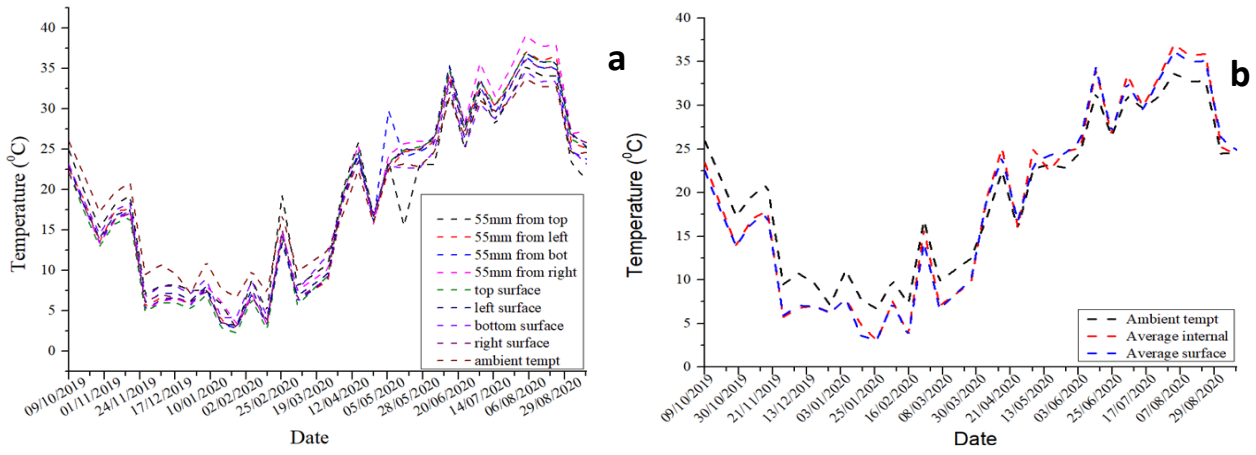

Fig. 5. Temperature variation of rubber composite sleeper under ambient conditions; (a) at different measuring points (internal and external), (b) average of internal and external

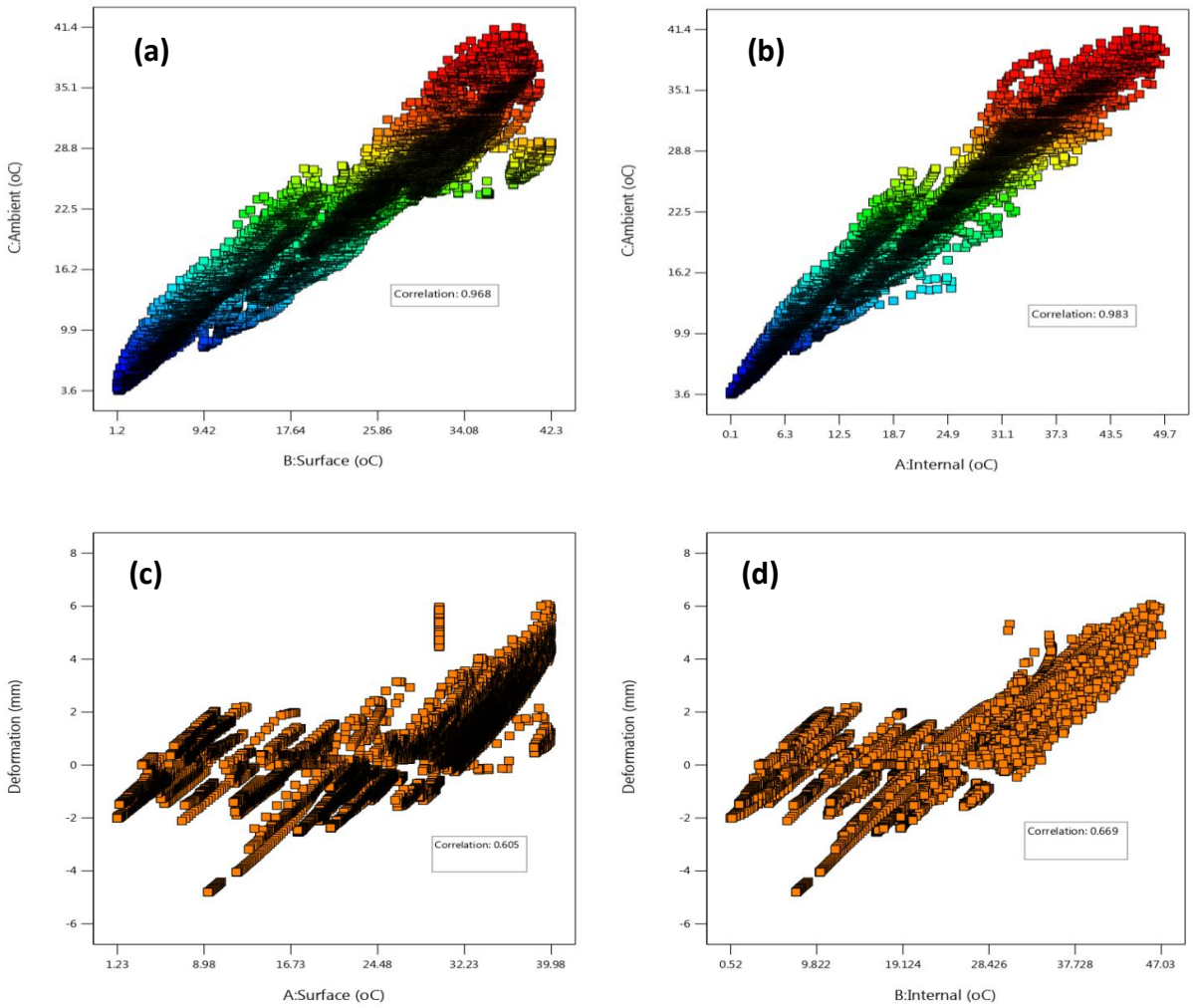

Fig. 6. Correlation analysis; (a) relationship between ambient and surface sleeper temperature, (b) relationship between ambient and internal sleeper temperature, (c) relationship between deformation and surface temperature, (d) relationship between deformation and surface temperature

The maximum positive and negative deformations of the rubber are approximately -0.67 and 0.9 mm in autumn, -0.32 and 0.25 mm in winter, -0.75 and 2.75 mm in spring, and -1.25 and 5.3 mm in summer. The maximum positive and negative deformations occurred at 16:30 and 17:30 hrs, and 7:30 to 10:30 hrs, respectively.

From the foregoing, it can be observed that most polymer materials, including those used in railway sleepers, exhibit significant thermal expansion when heated. This property means that as the polymer absorbs heat from sunlight, its volume increases. This expansion can lead to deformation if the increase in volume is constrained by adjacent materials or the sleeper's structural design. When the intensity of sunlight decreases, the polymer cools and contracts, potentially reversing some of the deformation.

3.3. Statistical modelling of sleeper temperature-dependent deformation using RSM

3.3.1. Model fitting

To establish the relationship between sleeper body temperature and deformation, regression analysis was conducted to determine the coefficients of model terms. Table 4 shows the ANOVA of the sleeper deformation predicted response surface model. The Table 4 shows the sum of squares, F-value, and P-value at the 0.05 significance level. The p-values less than 0.05 were used to evaluate the significance of each coefficient, thus indicating a desired agreement between the experimental and predicted results.

Based on Table 4, a quartic polynomial model was selected as the best to predict sleeper deformation. The model was selected based on the polynomial of the highest order in which additional terms are relevant and not aliased by the software. However, a stepwise model reduction was applied to the quartic model with p-values <0.05 to eliminate insignificant terms, and the reduced terms in the quartic model are presented in Table 4.

The results from Table 4 show that the quartic model with an F-value of 5674.45 and p-value <0.05 implies the model is significant, and there is only a 0.01% chance that an F-value this large could occur due to noise. The model terms (A, B, AB, A^2, B^2, AB^2, A^3, A^4) had p-values <0.05 which indicates that these terms significantly improve the model. The significance of the model terms reveals that the model terms have a synergistic effect on the regression model [36]. The Lack of Fit (LoF) F-value of 6.80 implies that the model is statistically fit as it is greater

than 0.05, as reported by Usman [42]. The final model equation for the deformation of the rubber composite sleeper is illustrated in Equation (16).

$$-2.94 - 0.61A + 1.45B - 0.045AB - 0.020A^2 - 0.013B^2 + 0.000512AB^2 + 0.0022A^3 - 0.000028A^4 \quad (16)$$

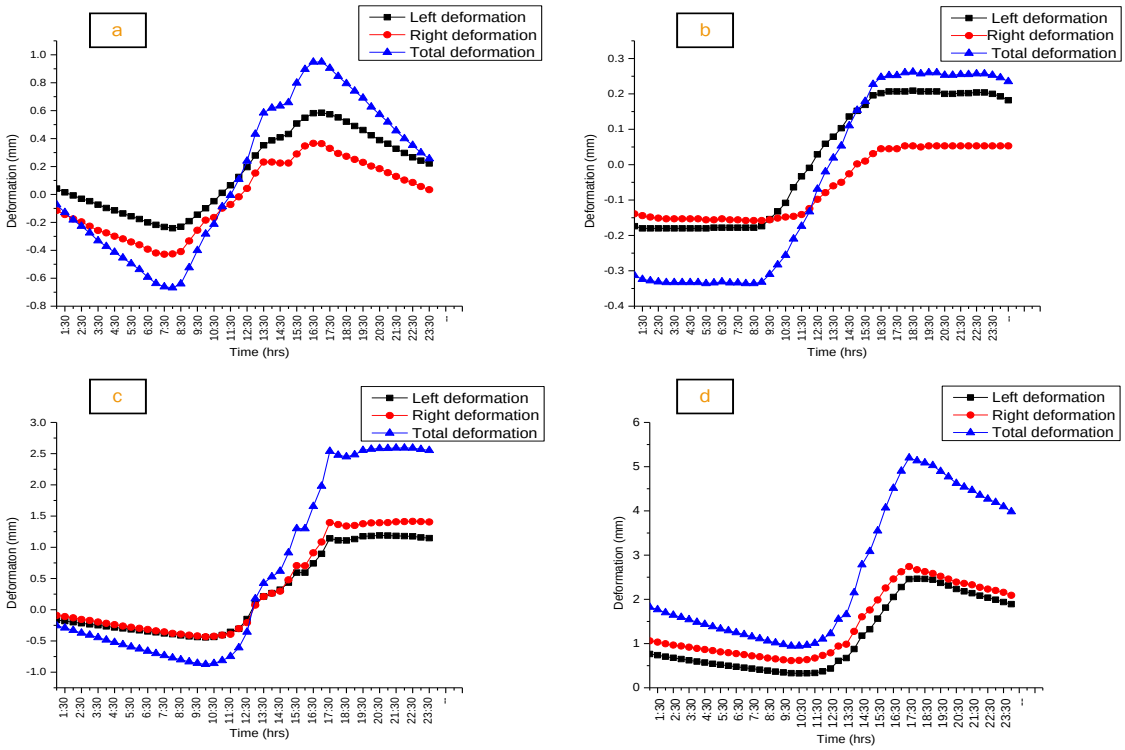

Fig. 7. Daily changes in the vertical temperature of rubber composite; (a) Summer, (b) Spring, (c) Winter, (d) Autumn

Table 4. ANOVA results for responses

Source	Sum of Squares	df	Mean Square	F-value	p-value	
Model	22217.55	8	2777.19	5674.45	< 0.0001	Significant
A-Surface	1599.97	1	1599.97	3269.11	< 0.0001	
B-Internal	1644.98	1	1644.98	3361.07	< 0.0001	
AB	322.64	1	322.64	659.24	< 0.0001	
A^2	1516.70	1	1516.70	3098.97	< 0.0001	
B^2	18.35	1	18.35	37.49	< 0.0001	
AB^2	189.38	1	189.38	386.95	< 0.0001	
A^3	18.49	1	18.49	37.78	< 0.0001	
A^4	768.29	1	768.29	1569.79	< 0.0001	
Residual	5187.86	10600	0.4894			
Lack of Fit	5164.36	10282	0.5023	6.80	< 0.0001	Significant
Pure Error	23.50	318	0.0739			
Cor Total	27405.41	10608				

3.3.2. RSM validation of model

In the RSM interpretation of model results, an adequate precision (the signal-to-noise ratio) greater than 4 is the desirable measure. The adequate precision of 444.760 obtained from the analysis indicates a strong signal. Thus, this model can be used to navigate the design. The deformation model regression was evaluated using the coefficient of determination, R^2 which gave a high value of 0.8107 from the ANOVA results presented in Table 5. The high R^2 indicates a good agreement between the experimental measurement and predicted calculations.

Table 5. ANOVA results for response

Std. Dev.	Mean	C.V. %	R^2	Adjusted R^2	Predicted R^2	Adeq Precision
0.6996	9.17	127.13	0.8202	0.8201	0.8197	444.760

Furthermore, the Predicted R^2 of 0.8197 is in reasonable agreement with the Adjusted R^2 of 0.8201, i.e., the difference is less than 0.2. From the foregoing, it can be deduced that the model presents an explicit type of relationship between the sleeper's body temperature (independent variable) and deformation (dependent variable).

3.3.3. Verification of model adequacy

The normal plot of residuals and the plot of actual versus predicted values of the sleepers' deformation were used to verify the adequacy of the model adopted, and the results are presented in Fig. 8(a) and 8(b). Fig. 8(a) shows a normal plot of residuals of the sleepers' deformation that

almost lies on the inclined straight line, which implies that the assumption of normal distribution is satisfied. The plot of actual versus predicted values in Fig. 8(b) also shows that almost all the values spread around the inclined straight line (equality line), which indicates that the prediction of the model is quite adequate as the actual and calculated deformations agree closely.

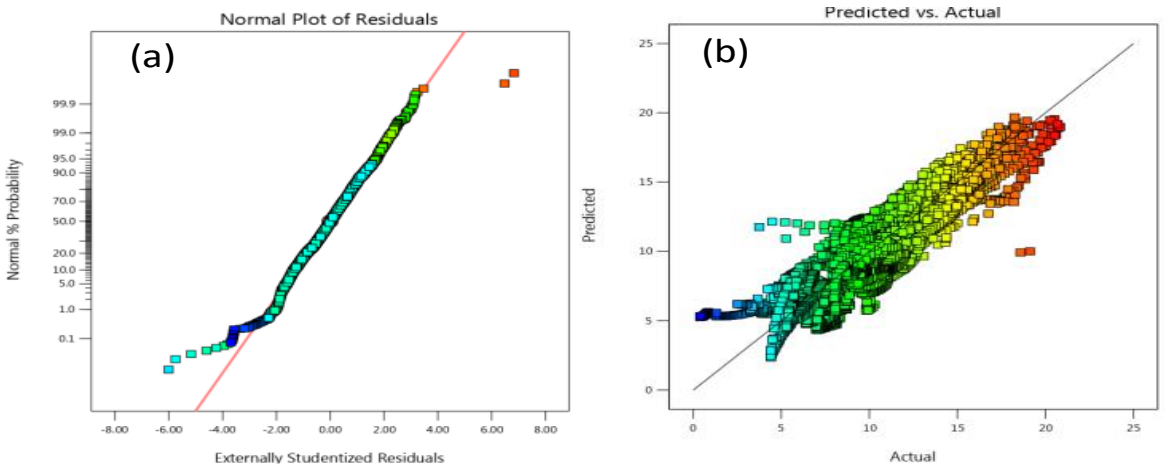

Fig. 8. Deformation response plot; (a) Externally studentized residual versus predicted deformation, (b) predicted versus actual plot

3.3.4. The interactive effect of internal and external temperature on deformation

The interactive effect of the two independent variables (internal and external sleeper temperature) on the response (deformation) in 2-D and 3-D.

The 2-D contour plot presented in Fig. 9(a) shows that overall contour lines are semi-elliptical in shape and most of the observation points lie around the equality, suggesting a very strong relationship between the internal and surface variables (model input variables).

Moreover, the result showed that the deformation of the sleepers increases as both internal and surface temperatures increase. For the surface temperature, however, the most deformation occurred around 32.23^{o}C – 39.98 ^{o}C, corresponding to an internal temperature of 28.4^{o}C – 47.03 ^{o}C. The 3-D result from Fig. 9(b) shows the deformation response of the sleepers to temperature. The blue region shows the area with decreased deformation (i.e., contraction), and the red region shows the sleeper area with increased deformation (i.e., expansion). This revealed that the deformation of the sleeper is more sensitive to changes in internal temperature than surface temperature. As the internal temperature rises, the atoms within the material gain energy, which enhances their mobility. The increased mobility allows the atoms to rearrange and glide past each other, leading to a change in shape. Moreover, the result showed that surface temperature from 30.3 – 39.98^{o}C and internal temperature from 23.8 – 47.03^{o}C leads to expansion in the sleepers, while surface temperature from 1.23 – below 39.98^{o}C and internal temperature from 0.52 – below 23.8^{o}C leads to contraction in the sleepers.

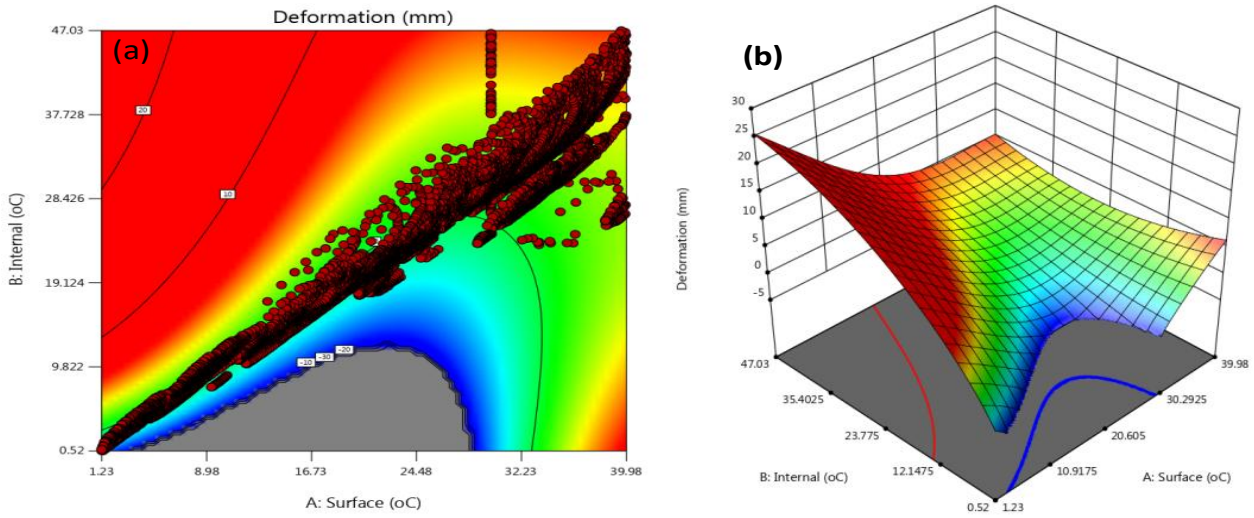

Fig. 9. Contour Plot of Sleepers Deformation; (a) 2-Dimensional, (b) 3- Dimensional

3.4. Machine learning techniques model evaluation (basic model)

To obtain the results of the basic model for XGBoost, CatBoost, KNN, and RF regressions, the default settings were employed and evaluated via accuracy and error metrics. The result is shown in Table 6.

Evaluating the performance of the basic model for the various machine learning techniques as shown in Table 6, based on the R2 and the error metrics values, revealed that the KNN outperformed other machine learning techniques by presenting the highest R2 value and lowest error metrics. However, all the machine learning algorithms presented high values of the R^2 and low values of MSE, MAE and RMSE indicating that

they are all capable of predicting the rubber composite sleeper deformation with high accuracy. Although all the different algorithms yielded good results with reasonable accuracy, an improvement was sought and applied to each model via a gridsearch algorithm capable of combining different hyperparameters to enhance the performance of the basic model. Consequently, the results of the improved models are presented as follows. The performance of the optimized model is presented in Table 7. The optimized hyperparameters that gave the best results have been presented earlier in the method section.

Table 6. Comparison of ML model performance metrics (Basic model)

S/n	Model	R^2	MSE	RMSE	MAE
1	Random forest	0.884	0.298	0.546	0.366
2	XGBoost	0.891	0.279	0.528	0.371
3	CatBoost	0.898	0.263	0.513	0.371
4	K nearest Neighbors	0.899	0.259	0.501	0.342

Table 7. Comparison of model performance metrics (optimized model)

S/n	Model	R^2	MSE	RMSE	MAE
1	Random forest	0.943	0.148	0.385	0.267
2	XGBoost	0.928	0.186	0.431	0.325
3	CatBoost	0.858	0.369	0.607	0.463
4	K nearest Neighbors	0.999	0.000258	0.016	0.000896

From Table 7, it can be observed that the R^2 values for all the algorithms tend to be improved with the optimization of the algorithms while the error margin decreases. Similar to the basic model, the optimized model results indicate that all the algorithms can predict the deformation of rubber composite sleepers with high accuracy. However, the KNN demonstrated the best predictive power with R^2 value of 0.99 and MSE, RMSE and MAE values of 0.000258, 0.016, and 0.000896 respectively. Although the basic model had the potential to predict the deformation of rubber composite sleepers with a reasonable level of precision, the predictive power of the models was improved using Gridsearch optimization.

Fig. 10 evaluated the predictive potential of the different ML algorithms to predict sleeper deformation. In Fig. 10(a-d), the correlation coefficient values of the RF, CatBoost, XGBoost, and KNN are 0.96, 0.95, 0.96, and 0.96 respectively, which indicates that the actual and predicted deformation of the rubber composite sleeper have a very strong positive relationship. To investigate the relationship between the actual and predicted deformation of the rubber composite sleeper, the point-to-point relative deformation was plotted and displayed in Fig. 11. The results indicate that all algorithms predicted the sleeper's deformation with minimal error margins. Also, the performance evaluation metrics of the different machine learning algorithms were explored and presented in Fig. 12. The result further proved that the KNN algorithm best predicts the temperature-dependent deformation of rubber composite sleepers by presenting the highest R^2 and lowest RSME, MSE, and MAE values.

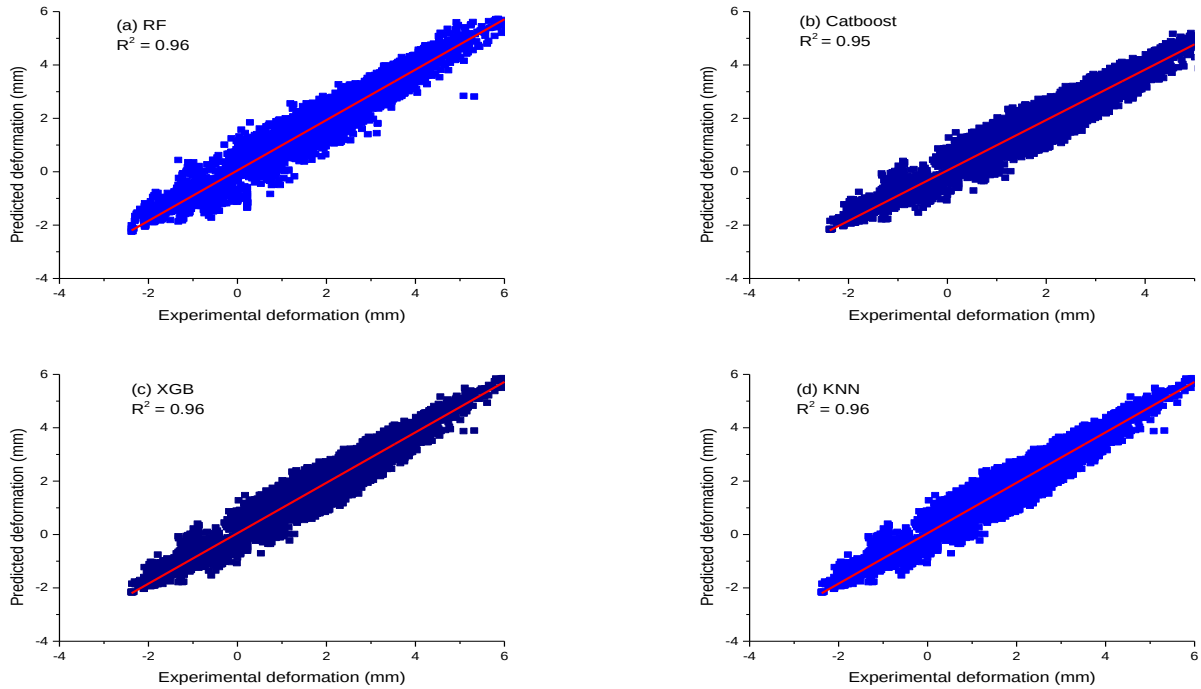

Fig. 10. Scatter plots of predicted sleeper deformation compared to sleeper deformation using different models algorithms; (a) RF, (b) Catboost, (c) XGBoost, (d) KNN

Fig. 11. Performance plot of experimental and predicted deformation with error margin; (a) RF, (b) Catboost, (c) XGBoost, (d) KNN

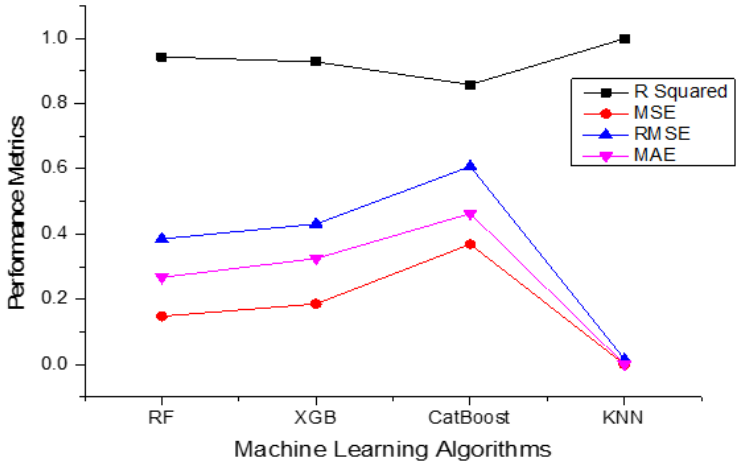

Fig. 12. Model Performance evaluation criteria (R^2, MAE, MSE and RMSE) for different algorithms

Table 8 compares the machine learning algorithms with the response surface methodology. The results obtained revealed that all the prediction algorithms employed in this study can predict sleeper deformation from temperature data with a very high level of accuracy with R^2 above 80% and low error metrics. It is worth noting that the KNN machine learning algorithm outperformed the other ML algorithms and the RSM.

Table 8. Comparison of ML algorithms model performance with RSM

S/n	Model	R^2	MSE	RMSE	MAE
1	Response surface methodology	0.820	1.788	1.337	1.0527
2	Random forest	0.943	0.148	0.385	0.267
3	XGBoost	0.928	0.186	0.431	0.325
4	CatBoost	0.858	0.369	0.607	0.463
5	K nearest Neighbors	0.999	0.000258	0.016	0.000896

6. Conclusion

The study attempted to develop a novel rubber composite sleeper-temperature deformation model using a designed measuring system to collect sleeper body temperature and its corresponding deformation over one year. Based on the data obtained, the models were developed and compared using the response surface methodology, RF, CatBoost, XGBoost, and KNN model regressions. These algorithms have not been used to predict the temperature-dependent deformation of rubber composite sleepers previously. The RSM was executed using Design Expert version 13 software, while ML was executed in Python programming language. The dataset in this study for ML was split into two fractions for training (70%) and testing (30%). The data was cleaned and normalized for the accuracy of the prediction model. The following are the conclusions deduced from the study.

- The temperature field on the sleeper surface body (Internal and surface) displayed a very similar and consistent changing trend with the ambient temperature. Thus, in the absence of sleeper body temperature or where there is a need to obtain quick reliable deformation of the rubber composite sleeper without the need for long-term experimentation, the ambient temperature present in the metrological stations can be relied upon to provide a highly accurate prediction of sleeper deformation. Also, there is a very strong correlation (above 96%) between the surface/internal temperature and the ambient temperatures, while a fair correlation (about 60%) exists between the surface/internal temperature field and the deformation.
- The maximum positive and negative deformations occurred at 16:30 and 17:30 hrs and 7:30 to 10:30 hrs, respectively. This implies that, like most polymer materials, the railway sleepers exhibit significant thermal expansion when heated. This property means that as the polymer absorbs heat from sunlight, its volume increases. This expansion can lead to deformation if the increase in volume is constrained by adjacent materials or the sleeper's structural design. When the intensity of sunlight decreases, the polymer cools and contracts, potentially reversing some of the deformations.
- The K-nearest neighbor algorithm outperformed the response surface method, XGBoost, CatBoost, and random forest algorithms by presenting the highest correlation coefficient and lowest error metrics; R^2, MSE, RMSE, and MAE values of 0.999, 0.000258, 0.016, and 0.000896 respectively. However, it is worth noting that all the methods employed to predict the deformation of rubber composite sleepers performed very well with a high degree of accuracy (R^2 value of greater than 80%).
- Although KNN proved to be the best fit for the prediction of the deformation of rubber composite sleepers, the independent/explanatory variables utilized in this study to predict the deformation of rubber composite sleepers are the internal and surface temperatures. It is worth noting that since there is a close relationship between the sleeper temperatures and the ambient, then the ambient temperature from metrological centres can be utilized as input variables. Also, it is therefore recommended that more variables such as wind speed, humidity, solar irradiation etc should be included as explanatory variables for more realistic predictions.
- The prediction models attempted in the study are cardinal in predicting failures or maintenance needs of the rubber composite sleeper in service. This enables proactive maintenance schedules, reducing downtime and costs, thus, allowing for timely maintenance interventions by railway practitioners.

Acknowledgement

The work described here was supported by the Natural Science Foundation of Hunan Province, China (Grant 2019JJ40384).

References

[1] É. A. Silva, D. Pokropski, R. You, and S. Kaewunruen, "Comparison of structural design methods for railway composites and plastic sleepers and bearers," Australian journal of structural engineering, vol. 18, no. 3, pp. 160-177, 2017. https://doi.org/10.1080/13287982.2017.1382045.

[2] W. Ferdous, A. Manalo, T. Aravinthan, and A. Remennikov, "Recent developments and applications of composite railway sleepers," CORE 2016: Maintaining the Momentum, p. 197, 2016.https://search.informit.org/doi/10.3316/informit.428799011790553.

[3] A. Ghorbani and S. Erden, "Polymeric composite railway sleepers," Sci. Rep, vol. 6, pp. 9-11, 2013.

[4] W. Ferdous, T. Aravinthan, A. Manalo, and G. Van Erp, "Composite railway sleepers: New developments and opportunities," in Proceedings of the 11th International Heavy Haul Association Conference (IHHA 2015), 2015: International Heavy Haul Association, pp. 1-9.

[5] I. Lotfy, M. Farhat, M. A. Issa, and M. Al-Obaidi, "Flexural behavior of high-density polyethylene railroad crossties," Proceedings of the Institution of Mechanical Engineers, Part F: Journal of Rail and Rapid Transit, vol. 230, no. 3, pp. 813-824, 2016, https://doi.org/10.1177/0954409714565655.

[6] W. Ferdous and A. Manalo, "Failures of mainline railway sleepers and suggested remedies–review of current practice," Engineering Failure Analysis, vol. 44, pp. 17-35, 2014, https://doi.org/10.1016/j.engfailanal.2014.04.020.

[7] Y. Pang, S. N. Lingamanaik, B. K. Chen, and S. F. Yu, "Measurement of deformation of the concrete sleepers under different support conditions using non-contact laser speckle imaging sensor," Engineering Structures, vol. 205, p. 110054, 2020/02/15/ 2020, doi: https://doi.org/10.1016/j.engstruct.2019.110054, https://doi.org/10.1016/j.engstruct.2019.110054.

[8] S. Kaewunruen, R. You, and M. Ishida, "Composites for timber-replacement bearers in railway switches and crossings," Infrastructures, vol. 2, no. 4, p. 13, 2017, https://doi.org/10.3390/infrastructures2040013.

[9] V. I. Kondrashchenko, G. Q. Jing, and C. Wang, "Wood-polymer composite for the manufacture of sleepers," in Materials Science Forum, 2019, vol. 945: Trans Tech Publ, pp. 509-514, https://doi.org/10.4028/www.scientific.net/MSF.945.509.

[10] W. Ferdous, A. Manalo, G. Van Erp, T. Aravinthan, S. Kaewunruen, and A. Remennikov, "Composite railway sleepers–Recent developments, challenges and future prospects," Composite Structures, vol. 134, pp. 158-168, 2015, https://doi.org/10.1016/j.compstruct.2015.08.058.

[11] E. Ferro, J. Harkness, and L. Le Pen, "The influence of sleeper material characteristics on railway track behaviour: concrete vs composite sleeper," Transportation Geotechnics, vol. 23, p. 100348, 2020, https://doi.org/10.1016/j.trgeo.2020.100348.

[12] G. Van Erp and M. Mckay, "Recent Australian developments in fibre composite railway sleepers," Electronic Journal of Structural

Engineering, vol. 13, no. 1, pp. 62-6, 2013, https://doi.org/10.56748/ejse.131611.
[13] E. R. Anne, "Rubber/plastic composite rail sleepers," UK: The waste & resources action programme, 2006.
[14] P. Chow, "Test report on mechanical properties with eight integrico composite crossties," Urbana, USA: University of Illinois, 2007.
[15] P. Cromberge, "Polymer rail sleepers being tested for the mining industry," Mining Weekly, 2005.
[16] C. Pattamaprom, D. Dechojarassri, C. Sirisinha, and W. Kanok-Nukulchai, "Natural rubber composites for railway sleepers: A feasibility study," Thammasat University, Thailand, 2005.
[17] G. Graebe, J. Woidasky, and J. Fraunhofer, "Railway sleepers from mixed plastic waste-Railwaste project status information," Fraunhofer ICT, 2010.
[18] S. Kaewunruen, "Acoustic and dynamic characteristics of a complex urban turnout using fibre-reinforced foamed urethane (FFU) bearers," in Noise and Vibration Mitigation for Rail Transportation Systems: Springer, 2015, pp. 377-384, https://doi.org/10.1007/978-3-662-44832-8_45.
[19] W. Ferdous et al., "Composites for alternative railway sleepers," in EASEC16: Springer, 2021, pp. 267-276, https://doi.org/10.1007/978-981-15-8079-6_26.
[20] A. S. Shanour, A. A. Khalil, H. S. Riad, and H. M. Bakry, "Experimental and analytical investigations of innovative composite materials using GFRP and iron slag for railway sleepers," J. Eng. Res. Reports, pp. 25-42, 2020.
[21] Z. Zeng, A. A. Shuaibu, F. Liu, M. Ye, and W. Wang, "Experimental study on the vibration reduction characteristics of the ballasted track with rubber composite sleepers," Construction and Building Materials, vol. 262, p. 120766, 2020, https://doi.org/10.1016/j.conbuildmat.2020.120766.
[22] Z. Zeng, A. A. Qahtan, G. Hu, R. Xu, and A. A. Shuaibu, "Comparative experimental investigation of the vibration mitigation characteristics of ballasted track using the rubber composite sleeper and concrete sleeper under various interaction forces," Engineering Structures, vol. 275, p. 115243, 2023, https://doi.org/10.1016/j.engstruct.2022.115243.
[23] Zeng, Z., Ye, M., Wang, W., Liu, J., Shen, S. and Qahtan, A.A.S., 2022. Analysis on mechanical characteristics of CRTSII slab ballastless track structures in rectification considering material brittleness. Construction and Building Materials, 319, p.126058, https://doi.org/10.1016/j.conbuildmat.2021.126058.
[24] Z. Zhao, Y. Gao, and C. Li, "Research on the Vibration Characteristics of a Track's Structure Considering the Viscoelastic Properties of Recycled Composite Sleepers," Applied Sciences, vol. 11, no. 1, p. 150, 2021, https://doi.org/10.3390/app11010150.
[25] Zhao, Z., Shen, Y., Wei, Q., Jiang, W., Geng, H. and Li, C., 2019. Experimental study on dynamic performance of composite sleeper ballasted track. J. Cent. South Univ. Sci. Technol, 50, pp.234-240, doi: 10.11817/j.issn.1672-7207.2019.01.029.
[26] M. A. Jabu, A. Alugongo, and N. Nkomo, "An Experimental Investigation on Effect of Rubber Particle Size on Composite Railway Sleeper Mechanical Strength and Vibrational Damping Properties.", International Journal of Engineering Trends and Technology, 72(2), 222-229, February 2024, https://doi.org/10.14445/22315381/IJETT-V72I2P123.
[27] Z. Zhao, Y. Gao, and C. Li, "Experimental Study on Dynamic Properties of a Recycled Composite Sleeper and Its Theoretical Model," Symmetry, vol. 13, no. 1, p. 17, 2021, https://doi.org/10.3390/sym13010017.
[28] V. Lojda, A. van Belkom, and H. Krejčiříková, "Investigation of the elastic modulus of polymer sleepers under a quasistatic and cyclic loading," Civil and Environmental Engineering, vol. 15, no. 2, pp. 125-133, 2019, DOI: 10.2478/cee-2019-0016.
[29] I. Lotfy, M. Farhat, and M. A. Issa, "Effect of pre-drilling, loading rate and temperature variation on the behavior of railroad spikes used for high-density-polyethylene crossties," Proceedings of the Institution of Mechanical Engineers, Part F: Journal of Rail and Rapid Transit, vol. 231, no. 1, pp. 44-56, 2017, https://doi.org/10.1177/0954409715620755.
[30] P. Yu et al., "Investigation on the physical, mechanical and microstructural properties of epoxy polymer matrix with crumb rubber and short fibres for composite railway sleepers," Construction and Building Materials, vol. 295, p. 123700, 2021, https://doi.org/10.1016/j.conbuildmat.2021.123700.
[31] M. Siahkouhi, X. Li, V. L. Markine, and G. Jing, "Experimental and numerical study on the mechanical behavior of Kunststof Lankhorst Product (KLP) sleepers," Scientia Iranica, 28(5), pp.2568-2581, 2021, https://doi.org/10.24200/sci.2021.57165.5096.
[32] C. Salih et al., "Novel Bending Test Method for Polymer Railway Sleeper Materials," Polymers, vol. 13, 2021, https://doi.org/10.3390/polym13091359.
[33] Z. Zeng, Z. Huang, H. Yin, X. Meng, W. Wang, and J. Wang, "Influence of track line environment on the temperature field of a double-block ballastless track slab," Advances in Mechanical Engineering, vol. 10, no. 12, p. 1687814018812325, 2018, https://doi.org/10.1177/1687814018812325.
[34] X. Chen, Y. Zhang, and P. Ge, "Prediction of concrete strength using response surface function modified depth neural network," (in eng), PloS one, vol. 18, no. 5, p. e0285746, 2023, doi: 10.1371/journal.pone.0285746.
[35] T. Awolusi, O. Oke, O. Akinkurolere, and A. Sojobi, "Application of response surface methodology: Predicting and optimizing the properties of concrete containing steel fibre extracted from waste tires with limestone powder as filler," Case studies in Construction materials, vol. 10, p. e00212, 2019, https://doi.org/10.1016/j.cscm.2018.e00212.
[36] M. H. Osman et al., "Response surface methodology optimization of concrete strength using hydroxyapatite nanopowder as admixture," Progress in Engineering Application and Technology, vol. 1, no. 1, pp. 134-141, 2020.
[37] D. Sinkhonde, R. O. Onchiri, W. O. Oyawa, and J. N. Mwero, "Response surface methodology-based optimisation of cost and compressive strength of rubberised concrete incorporating burnt clay brick powder," Heliyon, vol. 7, no. 12, p. e08565, 2021,https://doi.org/10.1016/j.heliyon.2021.e08565.
[38] I. K. Harith, M. J. Hussein, and M. S. Hashim, "Optimization of the synergistic effect of micro silica and fly ash on the behavior of concrete using response surface method," Open Engineering, vol. 12, no. 1, pp. 923-932, 2022, https://doi.org/10.1515/eng-2022-0332.
[39] S. A. Nwose, F. Edoziuno, and S. Osuji, "Statistical analysis and Response Surface Modelling of the compressive strength inhibition of crude oil in concrete test cubes," Algerian Journal of Engineering and Technology, vol. 4, pp. 99-107, 2021, http://dx.doi.org/10.5281/zenodo.4696030.
[40] Y. Gong, J. Song, S. Lin, J. Yang, Y. He, and G. Tan, "Design optimization of rubber-basalt fiber-modified concrete mix ratios based on a response surface method," Applied Sciences, vol. 10, no. 19, p. 6753, 2020, https://doi.org/10.3390/app10196753.
[41] Sinkhonde, David, Richard Ocharo Onchiri, Walter Odhiambo Oyawa, and John Nyiro Mwero. "Behaviour of rubberised concrete with waste clay brick powder under varying curing conditions." Heliyon, 9(2), (2023, https://doi.org/10.1016/j.heliyon.2023.e13372.
[42] A. Usman, M. H. Sutanto, M. Napiah, S. E. Zoorob, N. S. A. Yaro, and M. I. Khan, "Comparison of performance properties and prediction

of regular and gamma-irradiated granular waste polyethylene terephthalate modified asphalt mixtures," Polymers, vol. 13, no. 16, p. 2610, 2021, https://doi.org/10.3390/polym13162610.

[43] N. S. A. Yaro et al., "Modeling and optimization of rheological properties and aging resistance of asphalt binder incorporating palm oil mill waste using response surface methodology," Journal of Infrastructure Intelligence and Resilience, vol. 2, no. 1, p. 100026, 2023, https://doi.org/10.1016/j.iintel.2023.100026.

[44] T. B. Moghaddam, M. Soltani, M. R. Karim, and H. Baaj, "Optimization of asphalt and modifier contents for polyethylene terephthalate modified asphalt mixtures using response surface methodology," Measurement, vol. 74, pp. 159-169, 2015, https://doi.org/10.1016/j.measurement.2015.07.012.

[45] A. Rema and A. K. Swamy, "Response Surface–Based Approach to Quantify Variability in Recycled-Asphalt Concrete Mixtures," Journal of Materials in Civil Engineering, vol. 34, no. 11, p. 04022315, 2022, https://doi.org/10.1061/(ASCE)MT.1943-5533.0004479.

[46] J. Pagaimo, H. Magalhães, J. Costa, and J. Ambrosio, "Derailment study of railway cargo vehicles using a response surface methodology," Vehicle System Dynamics, vol. 60, no. 1, pp. 309-334, 2022, https://doi.org/10.1080/00423114.2020.1815810.

[47] J. Wang, S. Chen, X. Li, and Y. Wu, "Optimal rail profile design for a curved segment of a heavy haul railway using a response surface approach," Proceedings of the Institution of Mechanical Engineers, Part F: Journal of Rail and Rapid Transit, vol. 230, no. 6, pp. 1496-1508, 2016/08/01 2015, doi: 10.1177/0954409715602513.

[48] Shi, J., Gao, Y., Long, X. and Wang, Y., Optimizing rail profiles to improve metro vehicle-rail dynamic performance considering worn wheel profiles and curved tracks. Structural and Multidisciplinary Optimization, 63, pp.419-438, 2021, https://doi.org/10.1007/s00158-020-02680-7.

[49] S. Liu et al., "Deformation Analysis and Prediction of a High-Speed Railway Suspension Bridge under Multi-Load Coupling," Remote Sensing, vol. 16, no. 10, p. 1687, 2024, https://doi.org/10.3390/rs16101687.

[50] A. Ramos, A. Gomes Correia, K. Nasrollahi, J. C. O. Nielsen, and R. Calçada, "Machine Learning Models for Predicting Permanent Deformation in Railway Tracks," Transportation Geotechnics, vol. 47, p. 101289, 2024/07/01/ 2024, doi: https://doi.org/10.1016/j.trgeo.2024.101289.

[51] J. Chen et al., "A deep learning forecasting method for frost heave deformation of high-speed railway subgrade," Cold Regions Science and Technology, vol. 185, p. 103265, 2021/05/01/ 2021, doi: https://doi.org/10.1016/j.coldregions.2021.103265.

[52] S. Kaewunruen, J. Sresakoolchai, J. Huang, Y. Zhu, C. Ngamkhanong, and A. M. Remennikov, "Machine Learning Based Design of Railway Prestressed Concrete Sleepers," Applied Sciences, vol. 12, no. 20, p. 10311, 2022, https://doi.org/10.3390/app122010311.

[53] S. Hong, C. Park, and S. Cho, "A rail-temperature-prediction model based on machine learning: warning of train-speed restrictions using weather forecasting," Sensors, vol. 21, no. 13, p. 4606, 2021, https://doi.org/10.3390/s21134606.

[54] B. Indraratna, D. J. Armaghani, A. Gomes Correia, H. Hunt, and T. Ngo, "Prediction of resilient modulus of ballast under cyclic loading using machine learning techniques," Transportation Geotechnics, vol. 38, p. 100895, 2023/01/01/ 2023, doi: https://doi.org/10.1016/j.trgeo.2022.100895.

[55] P. Aela, J. Wang, K. Yousefian, H. Fu, Z.-Y. Yin, and G. Jing, "Prediction of crushed numbers and sizes of ballast particles after breakage using machine learning techniques," Construction and Building Materials, vol. 337, p. 127469, 2022, https://doi.org/10.1016/j.conbuildmat.2022.127469.

[56] S. Kako, "A Comparative Study about Accuracy Levels of Resistance Temperature Detectors RTDs Composed of Platinum, Copper, and Nickel," Al-Nahrain Journal for Engineering Sciences, vol. 26, pp. 216-225, 10/31 2023, doi: 10.29194/NJES.26030216.

[57] S. Hong et al., "Prediction of a representative point for rail temperature measurement by considering longitudinal deformation," Proceedings of the Institution of Mechanical Engineers, Part F: Journal of Rail and Rapid Transit, vol. 233, no. 10, pp. 1003-1011, 2019, https://doi.org/10.1177/0954409718822866.

[58] Fang, Xiu-Yang, Jian-En Gong, Feng Zhang, Hao-Nan Zhang, and Jia-Hong Wu. "Machine learning assisted materials design of high-speed railway wheel with better fatigue performance." Engineering Fracture Mechanics 292, 109586, 2023, https://doi.org/10.1016/j.engfracmech.2023.109586.

[59] I. Reis, D. Baron, and S. Shahaf, "Probabilistic random forest: A machine learning algorithm for noisy data sets," The Astronomical Journal, vol. 157, no. 1, p. 16, 2018, DOI 10.3847/1538-3881/aaf101.

[60] M. Savargiv, B. Masoumi, and M. R. Keyvanpour, "A new random forest algorithm based on learning automata," Computational Intelligence and Neuroscience, vol. 2021, 2021, https://doi.org/10.1155/2021/5572781.

[61] S. Hong et al., "Prediction of a representative point for rail temperature measurement by considering longitudinal deformation," Proceedings of the Institution of Mechanical Engineers, Part F: Journal of Rail and Rapid Transit, vol. 233, p. 095440971882286, 03/06 2019, doi: 10.1177/0954409718822866.

[62] Dang, Thanh Kim Mai, Mostafa Nikzad, Reza Arablouei, Syed Masood, Dac-Khuong Bui, Vi Khanh Truong, and Igor Sbarski. "Experimental study and predictive modelling of damping ratio in hybrid polymer concrete." Construction and Building Materials 411, 134541, 2024, https://doi.org/10.1016/j.conbuildmat.2023.134541.

[63] C. Lee and S. Lee, "Exploring the Contributions by Transportation Features to Urban Economy: An Experiment of a Scalable Tree-Boosting Algorithm with Big Data," Land, vol. 11, no. 4, p. 577, 2022. https://doi.org/10.3390/land11040577.

[64] T. Chen and C. Guestrin, "Xgboost: A scalable tree boosting system," in Proceedings of the 22nd acm sigkdd international conference on knowledge discovery and data mining, pp. 785-794, 2016, https://doi.org/10.1145/2939672.2939785.

[65] E. Okafor, D. O. Obada, Y. Ibrahim, and D. Dodoo-Arhin, "Prediction of the reflection intensity of natural hydroxyapatite using generalized linear model and ensemble learning methods," Engineering Reports, vol. 3, no. 2, p. e12292, 2021, https://doi.org/10.1002/eng2.12292.

[66] M. Kamran, B. Ullah, M. Ahmad, and M. M. S. Sabri, "Application of KNN-based isometric mapping and fuzzy c-means algorithm to predict short-term rockburst risk in deep underground projects," Frontiers in Public Health, vol. 10, p. 1023890, 2022, doi: 10.3389/fpubh.2022.1023890.

[67] P. T. Nguyen, "Application machine learning in construction management," TEM Journal, vol. 10, no. 3, pp. 1385-1389, 2021.

[68] S. C. Chelgani, H. Nasiri, A. Tohry, and H. Heidari, "Modeling industrial hydrocyclone operational variables by SHAP-CatBoost-A “conscious lab” approach," Powder Technology, vol. 420, p. 118416, 2023, https://doi.org/10.1016/j.powtec.2023.118416.

[69] Ahmad, Ayaz, Krzysztof Adam Ostrowski, Mariusz Maślak, Furqan Farooq, Imran Mehmood, and Afnan Nafees. "Comparative study of supervised machine learning algorithms for predicting the compressive strength of concrete at high temperature." Materials 14(15), 4222,

2021, https://doi.org/10.3390/ma14154222.
[70] J. T. Hancock and T. M. Khoshgoftaar, "CatBoost for big data: an interdisciplinary review," Journal of Big Data, vol. 7, no. 1, p. 94, 2020/11/04 2020, doi: 10.1186/s40537-020-00369-8.
[71] L. Prokhorenkova, G. Gusev, A. Vorobev, A. V. Dorogush, and A. Gulin, "CatBoost: unbiased boosting with categorical features," Advances in neural information processing systems, vol. 31, 2018.
[72] N. M. Shahani, M. Kamran, X. Zheng, C. Liu, and X. Guo, "Application of Gradient Boosting Machine Learning Algorithms to Predict Uniaxial Compressive Strength of Soft Sedimentary Rocks at Thar Coalfield," Advances in Civil Engineering, vol. 2021, p. 2565488, 2021/11/01 2021, doi: 10.1155/2021/2565488.
[73] V. Rathakrishnan, S. Bt. Beddu, and A. N. Ahmed, "Predicting compressive strength of high-performance concrete with high volume ground granulated blast-furnace slag replacement using boosting machine learning algorithms," Scientific Reports, vol. 12, no. 1, p. 9539, 2022/06/09 2022, doi: 10.1038/s41598-022-12890-2.
[74] D. Mohammadzadeh S, S.-F. Kazemi, A. Mosavi, E. Nasseralshariati, and J. H. Tah, "Prediction of compression index of fine-grained soils using a gene expression programming model," Infrastructures, vol. 4, no. 2, p. 26, 2019, https://doi.org/10.3390/infrastructures4020026.
[75] M. Hajihassani, S. S. Abdullah, P. G. Asteris, and D. J. Armaghani, "A gene expression programming model for predicting tunnel convergence," Applied Sciences, vol. 9, no. 21, p. 4650, 2019, https://doi.org/10.3390/app9214650.
[76] M. F. Javed et al., "Applications of gene expression programming and regression techniques for estimating compressive strength of bagasse ash based concrete," Crystals, vol. 10, no. 9, p. 737, 2020, https://doi.org/10.3390/cryst10090737.
[77] F. Aslam et al., "Applications of gene expression programming for estimating compressive strength of high-strength concrete," Advances in Civil Engineering, vol. 2020, 2020, https://doi.org/10.1155/2020/8850535.
[78] S. Abdulrazaq, "Streamflow prediction in ungauged river basin using gene expression programming," Universiti Teknologi Malaysia, 2016.
[79] T. Chai and R. R. Draxler, "Root mean square error (RMSE) or mean absolute error (MAE)?–Arguments against avoiding RMSE in the literature," Geoscientific model development, vol. 7, no. 3, pp. 1247-1250, 2014, https://doi.org/10.5194/gmd-7-1247-2014.
[80] T. O. Hodson, "Root mean square error (RMSE) or mean absolute error (MAE): when to use them or not," Geoscientific Model Development Discussions, pp. 1-10, 2022, https://doi.org/10.5194/gmd-15-5481-2022.
[81] D. S. K. Karunasingha, "Root mean square error or mean absolute error? Use their ratio as well," Information Sciences, vol. 585, pp. 609-629, 2022/03/01/ 2022, doi: https://doi.org/10.1016/j.ins.2021.11.036.
[82] W. Wang and Y. Lu, "Analysis of the mean absolute error (MAE) and the root mean square error (RMSE) in assessing rounding model," in IOP conference series: materials science and engineering, 2018, vol. 324, no. 1: IOP Publishing, p. 012049, DOI 10.1088/1757-899X/324/1/012049.
[83] A. H. Gandomi, S. K. Babanajad, A. H. Alavi, and Y. Farnam, "Novel approach to strength modeling of concrete under triaxial compression," Journal of materials in civil engineering, vol. 24, no. 9, pp. 1132-1143, 2012, https://doi.org/10.1061/(ASCE)MT.1943-5533.0000494.
[84] A. Garcia Asuero, A. Sayago, and G. González, "The Correlation Coefficient: An Overview," Critical Reviews in Analytical Chemistry - CRIT REV ANAL CHEM, vol. 36, pp. 41-59, 01/01 2006, doi: 10.1080/10408340500526766.
[85] Sammut, Claude, and Geoffrey I. Webb, eds. Encyclopedia of machine learning. Springer Science & Business Media, 2011.
[86] Schneider, Patrick, and Fatos Xhafa. Anomaly detection and complex event processing over iot data streams: with application to EHealth and patient data monitoring. Academic Press, 2022.